Research on Long Stroke Moving Secondary Permanent Magnet Linear Eddy Current Brake

Baoquan Kou, *Member, IEEE*, He Zhang, Xiangrui Yin, Yiheng Zhou and Chunyan Li
(Invited)

***Abstract*—In this paper, a long stroke moving secondary permanent magnet linear eddy current brake is proposed. Without exciting coils, the permanent magnet eddy current brake possesses the advantage of saving copper and better reliability. The topology and operating principle are presented. The mathematical model was derived with the layer theory. The braking force characteristic was analyzed using the finite element method. The structural parameters of the long stroke moving secondary permanent magnet linear eddy current brake were studied by referring the design progress of the other types of eddy current brakes. Finally, a prototype of long stroke moving secondary permanent magnet linear eddy current brake was built and tested, and the experimental result verifies the correctness of the above analysis.**

***Index Terms*—Braking force analysis, eddy current brake, experimental study, mathematical model, permanent magnet.**

I. INTRODUCTION

WHEN a conductor moves relative to the magnetic field or is in a changing magnetic field, the induced current will generate in the conductor. The induced current is also called the eddy current. The eddy current often brings harmful results in many different applications, such as the eddy current in the iron core of motors and transformers which wastes a lot of energy, and the produced heat seriously affects the performance of equipment and even damages the equipment. On the other hand, the eddy current can also be used in some occasions and has excellent characteristics. For example, the eddy current brake (ECB) is an electromagnetic device based on the eddy current [1-5]. It can generate braking force by the interaction between the eddy currents and the magnetic field, and can be used to realize contactless braking.

An important application of the eddy current brake is the test of linear motion devices such linear motors and trains. With the rapid development of modern engineering technology, the research on various linear motion devices is increasing. At the same time, braking technology is a key technology in the research of these motion devices. At present, there are many braking methods for linear motion devices, but most of them are limited to the traditional sticky braking mode, which mainly uses contact friction between devices to produce braking force. The shortcomings of this braking mode are obvious, which is greatly restricted by the contact surface conditions and the surrounding environment, and it also produces more serious noise and dust pollution, and the reliability is not high. On the other hand, the contact braking makes the braking components worn or damaged easily, and the repeated test cost is high; moreover, it produces greater impact and vibration in the braking process, which is sensitive to measuring instruments. Accuracy will affect, even damage the measuring instrument, leading to the failure of the test. Correspondingly, eddy current braking is an effective non-adhesive braking mode, which has been widely used in recreational facilities, rail transit elevators and so on.

According to the field source, the eddy current brakes can be divided into electromagnetic eddy current braking, permanent magnet eddy current braking and hybrid eddy current braking. The electromagnetic eddy current braking has the disadvantages of large volume, large loss, high temperature of excitation winding and the danger of power failure. The permanent magnet eddy current braking overcomes the above shortcomings. It does not need additional excitation winding and power supply, and it has the advantages of compact structure, saving energy, high efficiency, low maintenance cost, long life, and high reliability [6-16]. Hybrid eddy current brake combines the advantages of both the electromagnetic eddy current braking and permanent magnet eddy current braking, but its structure is more complex, and there is also the risk of power failure [17-19].

This paper presents a long stroke moving secondary permanent magnet linear eddy current brake. In Section II, the topology and operating principle are presented. In Section III, the formulas of the magnetic field and braking force are provided by using the layer theory. Then, the relationship between braking force and structural parameters such as the dimensions of the permanent magnets and yoke are studied.

Manuscript was submitted for review on 25, January, 2019.

This work was supported in part by the National Natural Science Foundation of China under Grant 51877051, the Research and Development Project of Scientific and Technological Achievements in Provincial Universities of Heilongjiang Education Department under Grant TSTAU-C2018014.

Baoquan Kou is with the School of Electrical and Automation, Harbin Institute of Technology, Harbin, 150001 China (e-mail: koubqhit@ 163.com).

He Zhang is with the School of Electrical and Automation, Harbin Institute of Technology, Harbin, 150001 China (e-mail: antonyamanda@163.com).

Xiangrui Yin is with the School of Electrical and Automation, Harbin Institute of Technology, Harbin, 150001 China (e-mail: 15846342869 @163.com).

Yiheng Zhou is with the School of Electrical and Automation, Harbin Institute of Technology, Harbin, 150001 China (e-mail: sethvoler@163.com).

Chunyan Li is with the School of Mechanical and Electrical Engineering, Heilongjiang University, Harbin, 150001 China (e-mail: lichunyanlmm@163.com).

Digital Object Identifier 10.30941/CESTEMS.2019.00004

Finally, a prototype is designed and built. The braking force characteristic is tested to verity the analysis above.

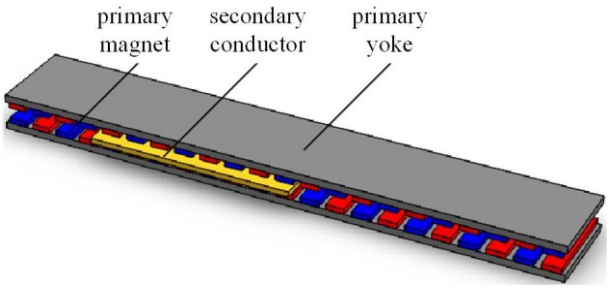

Fig. 1. Topology of the long stroke moving secondary permanent magnet linear eddy current brake.

II. Structure and Working Principle of Permanent Magnet Linear Eddy Current Brake

A. Structure of The Linear Eddy Current Brake

The long stroke moving secondary permanent magnet linear eddy current brake consists of a primary and a secondary. Fig. 1 and Fig. 2 shows its three dimensional (3-D) view and side view, respectively. The primary consists of two fixed primary structures, each is consisted of a flat primary core made of Steel_1010, and permanent magnets made of NdFeB35. The permanent magnets are magnetized perpendicular to the direction of movement and they are placed in notches with alternate polarity. The secondary is made of aluminum with high conductivity or composite materials with high conductivity and high permeability.

B. Working Principle of The Linear Eddy Current Brake

The magnetic field generated by primary permanent magnets will form a magnetic circuit in the primary iron core, air gap and secondary conductor. According to the law of electromagnetic induction, the relative movement of the primary permanent magnets and the secondary conductor plate causes eddy currents in the secondary conductor plate. Due to the circulation of eddy currents, an induced magnetic field is generated that interacts with the magnetic field generated by the primary permanent magnets, which results in a braking force between the primary and the secondary conductor.

III. Analytical Model

The analytical model of long stroke moving secondary permanent magnet linear eddy current brake is obtained based on the layer theory. The air gap magnetic field distribution and force characteristic equations are deduced, which provides a theoretical basis for the subsequent brake design.

A. Air Gap Magnetic Field Analysis

Fig. 2 shows the long stroke moving secondary permanent magnet linear eddy current brake model. When calculating the eddy current braking force of the conductor plate by layer method, the eddy current in the secondary conductor plate should be calculated first, and then the eddy current braking force can be obtained by the eddy current loss or Maxwell tensor method. Ignoring the edge effect, the model can be considered to be two dimensional, as shown in Fig. 2, the model

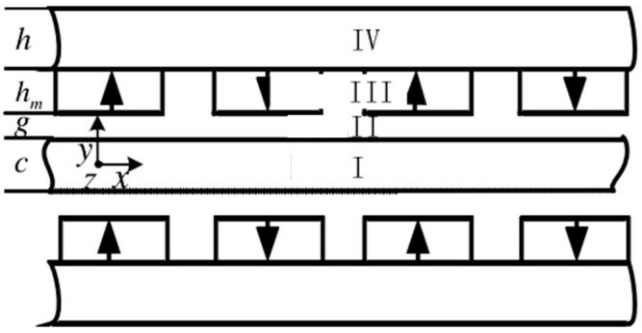

Fig. 2. The long stroke moving secondary permanent magnet linear eddy current brake model.

can be divided into four solving regions, each of which is distinguished by the following corner labels:

1) Region I : conductor plate layer, in which the eddy current is induced by the relative motion of the conductor plate and the primary layer.

2) Region II : air gap layer.

3) Region III : permanent magnet layer.

4) Region IV : primary magnet layer.

Where h is the height of primary iron core, h_m is the height of permanent magnets, g and c are the air gap length and conductor plate thickness, respectively.

In order to simplify the analysis, the following assumptions are made.

1) Assume that the primary and secondary are infinitely long in the x direction.

2) There is only eddy current in z direction in the conductor plate.

3) The air gap magnetic induction intensity is constant in z direction, regardless of the transverse end effect.

4) The relative permeability of the conductor plate and the permanent magnet is 1, and the conductivity of the conductor plate is constant.

5) The permeability of primary back iron is infinite and its conductivity is neglected, i.e. the eddy current effect is not considered.

Area I is a conductor plate layer. When the brake is working, eddy current will be induced in this layer. The eddy current density induced by the brake can be as high as that induced by the brake. From Ohm's Law:

$$J_1 = \sigma_1 E_1 \tag{1}$$

where J_1, σ_1, E_1 are the current, the conductivity and the electric field intensity of layer 1.

According to Ferrari's law of electromagnetic induction,

$$\nabla \times E_1 = -\frac{dB_1}{dt} = -\frac{dB_1}{dx}\frac{dx}{dt} = -\frac{dB_1}{dx}v \tag{2}$$

where v is the speed of the conductor plate, B_1 is the magnetic flux density of layer 1.

(2) cam be written as:

$$E_1 = -\frac{dA_1}{dx}v \tag{3}$$

where A_1 is the vector magnetic potential of layer 1.

In region I,

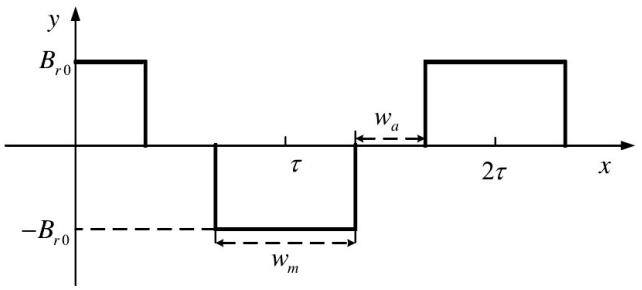

Fig. 3. The distribution of the permanent magnet remanence.

$$\nabla^2 A_1 = \mu_0 \sigma_1 v \frac{dA_1}{dx} \tag{4}$$

$$\frac{\partial^2 A_1}{\partial x^2} + \frac{\partial^2 A_1}{\partial y^2} = \mu_0 \sigma_1 v \frac{dA_1}{dx} \tag{5}$$

where μ_0 is the vacuum permeability.

In region II, the conductivity is zero. There is no current in this layer. Therefore, the vector potential equation of this layer is

$$\nabla^2 A_2 = 0 \tag{6}$$

$$\frac{\partial^2 A_2}{\partial x^2} + \frac{\partial^2 A_2}{\partial y^2} = 0 \quad 7)$$

In region III, which consists of the permanent magnets and air gap, and the permanent magnet is magnetized vertically, the distribution of magnetic flux density in this layer is as follows:

$$B_3 = \begin{pmatrix} B_{3x} \\ B_{3y} \\ B_{3z} \end{pmatrix} = \begin{pmatrix} 0 \\ B_r \\ 0 \end{pmatrix} - \mu_3 \begin{pmatrix} H_{3x} \\ H_{3y} \\ 0 \end{pmatrix} \tag{8}$$

$B_{r's}$ waveform is shown in Fig 3. Thus, the half-wave mirror rectangular wave can be expanded into Fourier series:

$$B_r(x) = \sum_n B_{r,n} e^{jnx}, n = 1,3,5,... \tag{9}$$

$$B_{r,n} = \frac{4B_{r0}}{n\pi} \sin\left(\frac{m w_m}{2}\right), m = \frac{n\pi}{\tau} \tag{10}$$

where τ, w_m, w_a are the pole distance, the length of permanent magnets in the moving direction, and the gap of adjacent permanent magnets along the moving direction.

The vector magnetic potential equation of this layer can be obtained as follows:

$$\frac{\partial^2 A_3}{\partial x^2} + \frac{\partial^2 A_3}{\partial y^2} = -\nabla \times B_3 \tag{11}$$

Region IV is the primary back iron layer. If the conductivity is neglected, there is no eddy current in the layer. The vector magnetic potential equation is:

$$\frac{\partial^2 A_4}{\partial x^2} + \frac{\partial^2 A_4}{\partial y^2} = 0 \tag{12}$$

Appling the connection condition of two adjacent contact surfaces and the boundary conditions, the solution of the vector magnetic potential of each layer is as follows:

$$A_{1,n}(x,y) = C_{1,n} e^{\lambda y + jmx} + D_{1,n} e^{-\lambda y + jmx} \tag{13}$$

$$A_{2,n}(x,y) = C_{2,n} e^{my + jmx} + D_{2,n} e^{-my + jmx} \tag{14}$$

$$A_{3,n}(x,y) = C_{3,n} e^{my + jmx} + D_{3,n} e^{-my + jmx} - jB_{r,n} e^{jmx} / m \tag{15}$$

$$A_{4,n}(x,y) = D_{4,n} e^{-my + jmx} \tag{16}$$

where $\lambda = \sqrt[4]{m^4 + (u_0 m \sigma_1 v)^2}\, e^{j\xi}$, $\xi = \frac{1}{2}\arctan\left(\frac{\mu_0 \sigma_1 v}{m}\right)$.

Because the secondary conductor plate is made of non-magnetic materials, the study of magnetic field is equivalent to air gap. In fact, the study of air gap magnetic field is mainly about the magnetic field in the conductor plate. From the last section, we can know the distribution of vector magnetic potential in the conductor layer, and the distribution of magnetic induction intensity in the conductor layer is as follows:

$$B_1 = \begin{pmatrix} \lambda D_1 e^{\lambda y + jmx} - \lambda D_1 e^{-\lambda y + jmx} \\ -jmD_1 e^{\lambda y + jmx} - jmD_1 e^{-\lambda y + jmx} \\ 0 \end{pmatrix} \tag{17}$$

The center line of the air gap, i. e. the middle plane of the conductor plate, is taken as a study in the plane. The magnetic induction intensity has only component in the *y* direction and periodically distributes along the *x* direction.

$$B_1(x) = \sum_n B_{1,n}(x) = \sum_n -j2mQ_n B_{1,n} e^{jmx} = \sum_n -\frac{m \sinh(mh_m)}{\lambda G} B_{r,n} e^{jmx} \tag{18}$$

The fundamental air gap magnetic field is

$$B_{1,1}(x) = B_{\delta,1} e^{j\pi x/\tau} = \frac{4B_{r0} \sinh(\pi h_m / \tau)}{\lambda \tau G} \cdot \sin\left(\frac{\alpha\pi}{2}\right) e^{j\pi x/\tau} \tag{19}$$

where α is the pole arc coefficient.

The amplitude of fundamental air gap magnetic density is:

$$B_{\delta,1} = \frac{4B_{r0} \sinh(\pi h_m / \tau)}{\lambda \tau G} \cdot \sin\left(\frac{\alpha\pi}{2}\right) \tag{20}$$

B. Braking Force Analysis

As when the brake operates, the eddy current is only induced in the conductor plate, and the eddy current losses are all in theory. The brake provides the braking force, so the eddy current loss method is used to solve the braking force.

The eddy currents generated in region I is,

$$J = \sum_n v\sigma_1 B_{1,n} = \sum_n j2mv\sigma_1 Q_n e^{jmx} \cosh \lambda y \tag{21}$$

It should be noticed that the eddy current induced in the conductor plate will gather in the conductor when the brake operates at a higher speed. The surface area of the body plate is affected by the skin effect of current. In engineering, the penetration depth is often used to represent field quantity of skin collection in conductors.

$$d_0 = \sqrt{\frac{2}{\omega \mu_0 \sigma_1}} \tag{21}$$

Therefore, the actual distribution depth of eddy current on one side of the conductor plate is as follows:

$$d_1 = \min(d_0, c/2) \tag{21}$$

It is proved that the skin effect of eddy current has little effect on the secondary structure eddy current brake in the middle and low speed section, because it can be considered as a simplified

analysis. The eddy current loss power is,

$$P_e = 2\frac{l_w}{2\sigma_1}\iint_{\text{Region1}} J\cdot J^* dxdy = \frac{l_w}{\sigma_1}\int_0^{d_1}\int_0^{l_c} J\cdot J^* dxdy \quad (21)$$

where l_w and l_c are the width of primary and the length of secondary conductor plate.

Considering the power loss of eddy current caused by the harmonic is as follows,

$$P_{en} = l_c l_w \sigma_1 v^2 m^2 \left|Q_n\right|^2 \left(\frac{\sinh(k_1 c)}{k_1} + \frac{\sinh(k_2 c)}{k_2}\right) \quad (22)$$

where $k_1 = q\cos\xi$, $k_2 = q\sin\xi$, $q = \sqrt[4]{m^4 + (\mu_0 m\sigma_1 v)^2}$.

The braking force is:

$$F_e = \frac{P_e}{v} = \frac{1}{4} l_c l_w \sigma_1 v B_{\delta 0}^2 \left|K_d\right|^2 \left(\frac{\sinh(k_1 c)}{k_1} + \frac{\sinh(k_2 c)}{k_2}\right) \quad (23)$$

From the expression of the braking force, it can be seen that the braking force is closely related to the size parameters, static air gap magnetic field and running speed of the brake, and is approximately proportional to the primary width and the length of the secondary conductor plate.

Longitudinal static end effect, also known as the first kind of longitudinal end effect, refers to the magnetic field distortion caused by the breaking of the primary two ends of linear motor. For linear induction motors, it results in the unequal mutual inductance of primary three-phase windings and asymmetric current, which leads to the distortion of magnetic field. This end effect is often neglected when the number of electrodes is large. The brake in this paper is a long primary and short secondary structure, so the effect of longitudinal static end effect is very small.

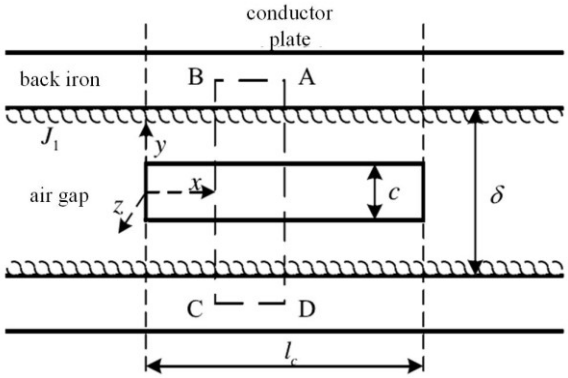

Fig. 4. The model of longitudinal dynamic end effect.

Longitudinal dynamic end effect is also called the second kind of longitudinal end effect. Generally speaking, for the short primary structure, it is caused by the sudden entry or departure of the secondary from the primary corresponding region. For the long-stroke brake studied in this paper, due to the breaking of the two ends of the secondary plate, the magnetic field at the two ends of the secondary plate will be distorted and additional braking power will be generated. In order to simplify the analysis process, the equivalent current layer analytical model is established, as shown in Fig. 4. The primary permanent magnet is replaced by an infinitely thin current layer which can generate the equivalent magneto-dynamic potential, and its surface current density.

The distribution of static air gap magnetic density is as follows:

$$B_\delta(x) = \sum_n B_{\delta,n} e^{jmx} = \sum_n -\frac{B_{r,n}\sinh mh_m}{\sinh m(g + h_m + c/2)} e^{jmx} \quad (24)$$

Assuming that the air gap magnetic field is uniformly distributed along the *y* direction, the second air gap coefficient is introduced here. K_{g2} compensates for the effect of the non-uniform distribution of the actual air gap magnetic field along the *y* direction:

$$K_{g2} = \frac{\sinh(\pi\delta/2\tau)}{\pi\delta/2\tau} \quad (25)$$

The equivalent electromagnetic air gap is

$$\delta_2 = K_{g2}\delta \quad (26)$$

According to the principle of equivalence, the magnetic field produced by the infinite thin current layer on the back iron surface in the air gap should be the same as the traveling wave magnetic field produced by the actual permanent magnet. Therefore, the surface current density of the infinite thin current layer can be assumed.

$$AT_1 = \sum_n \int_0^x J_{1n}\cos(mx)dx = -\sum_n \frac{J_{1n}}{m}\sin(mx) \quad (27)$$

The resulting air gap magnetic field is:

$$B_\delta = \frac{2\mu_0 AT_1}{\delta_2} \quad (28)$$

Applying Ampere Loop Law to the ABCD loop in Fig. 4, and considering $J_c = \sigma_1 v B_c$, the magnetic field is solved as:

$$B_c(x) = \frac{\beta_1}{m^2 + \alpha_1^2}\left(C_c e^{-\alpha_1 x} + m\sin(mx) + \alpha_1\cos(mx)\right) \quad (29)$$

where,

$$\alpha_1 = \frac{\mu_0\sigma_1 cv}{\delta_2}, \beta_1 = \frac{2\mu_0 J_{1n}}{\delta_2} \quad (30)$$

$$C_c = \frac{m^2 + \alpha_1^2}{\beta_1} B_{\delta n}\cos(mvt) - \alpha_1 \quad (31)$$

Thus,

$$B_c(x) = B_{\delta n}\cos(mvt)e^{-\alpha_1 x} - \frac{\alpha_1\beta_1}{m^2 + \alpha_1^2} e^{-\alpha_1 x} + \frac{\beta_1}{\sqrt{m^2 + \alpha_1^2}}\sin(mx + \arctan\frac{m}{\alpha_1}) \quad (32)$$

It can be seen from the above formula that the third term at the right end of the formula is the traveling wave magnetic field with a period of 2_in the conductor plate, the first term is the attenuation fluctuation of the magnetic field caused by the longitudinal dynamic edge effect, and the second term is the distortion of the magnetic field caused by the edge effect, which shows the weakening effect on the original magnetic field, thereby reducing the braking force of the brake.

The transverse static end effect, also known as the first kind of transverse end effect, is produced when the brake is stationary and the transverse distribution of air gap magnetic

field is not uniform. The analysis of the end effect can be further analyzed by conformal transformation. The third air gap coefficient is introduced as follows:

$$K_{g2}=\frac{1}{1+(1.594-1/66e^{-c/\delta_2})\delta_2/l_w} \tag{33}$$

The equivalent electromagnetic air gap is

$$\delta_3=K_{g3}\delta_2 \tag{34}$$

In the analytical process of the above two-dimensional model, it is assumed that the current in the secondary conductor plate exists only in the z-direction component, which is equivalent to assuming that the secondary plate is infinitely long along the z-direction. The actual length of the secondary conductor plate in Z direction is finite, which leads to the current component in X direction. This effect leads to the change of eddy current distribution in the conductor plate, which leads to the change of braking force. This kind of end effect is called transverse dynamic end effect, which is also called the second kind of transverse end effect. The analysis can be solved by Russell coefficient [20]:

$$K_n=1-\tanh\left(m\frac{l_w}{2}\right)\Big/m\frac{l_w}{2}(1+\gamma) \tag{35}$$

It can be considered to be equivalent to the secondary conductor plate to compensate, that is to say:

$$\sigma_1'=K_n\sigma_1 \tag{36}$$

Accordingly, a three-dimensional modified analytical model can be obtained on the basis of the two-dimensional analytical model.

In order to verify the accuracy of the air gap magnetic field in the second chapter analytical model, the force characteristic curves are compared.

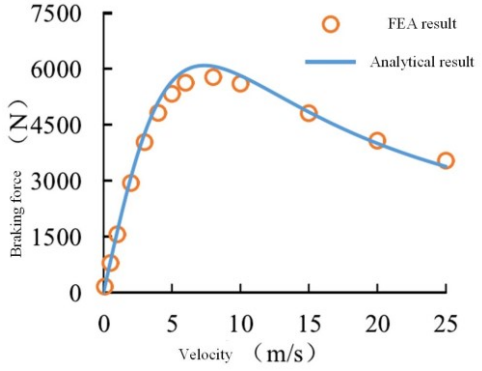

Fig. 5. Comparison of the FEA and analytical results.

From the force characteristic curve of the brake shown above, it can be seen that the force characteristic curve obtained by the analytical method is basically consistent with the results of the finite element simulation, which verifies the accuracy of the analytical model. However, there are still some deviations between the two. This is mainly due to the neglect of the influence of magnetic field high harmonics and magnetic leakage in the analytical model of permanent magnet linear eddy current brake, the neglect of the effect of core saturation, and the neglect of the effect of secondary conductor plate on finite length. At the same time, it can be seen that the normal force model of secondary eccentricity of brake also has high accuracy.

IV. Braking Force Analysis

Base on the theoretical analytical model and the finite element analysis model, the influence of the parameters such as the pole number, pole distance, size of permanent magnet and secondary plate on the braking performance is studied, so as to effectively improve the braking force density of the permanent magnet linear eddy current brake.

A. The Relation between Design Objectives and Main Structural Parameters

The main design objective of permanent magnet linear eddy current brake is high braking force density. The braking force density concerned here is the surface density of braking force, that is, the ratio of thrust amplitude to air gap area. So the eddy current braking force density is defined as,

$$f_e=\frac{F_e}{S_g}=\frac{F_e}{l_c l_w} \tag{37}$$

where S_g refers to the air gap area of brake.

For this kind of permanent magnet linear eddy current brake, it can be seen that in some cases, the greater the amount of permanent magnet used, the greater the braking force density. Therefore, it is necessary to determine a parameter to characterize the efficiency of permanent magnet to ensure that the permanent magnet can be used reasonably and effectively. In this paper, the braking force generated by the unit permanent magnet is considered to represent the utilization ratio of the permanent magnet, i.e. the unit permanent magnet power, which is defined as equation (38). In this paper, the unit permanent magnet power is used to help determine the size parameters of permanent magnets reasonably in the process of parameter optimization.

$$f_m=\frac{F_e}{V_m}=\frac{F_e}{2pl_w w_m h_m} \tag{38}$$

where V_m refers to the volume of magnets.

Because the permanent magnet linear eddy current brake is a long primary and short secondary structure, and the secondary conductor plate is relatively limited in length, the braking force produced by the brake fluctuates. The braking force volatility is defined here as follows:

$$\rho=\frac{F_{\max}-F_{\min}}{F_{avg}}\times 100\% \tag{39}$$

It is proved that harmonics have little effect on the brake force, so its fundamental wave amplitude is studied here. From (23) and (37), the braking force density is,

$$f_e=\frac{F_e}{l_c l_w}=\sigma_1 v m^2|Q_1|^2\left(\frac{e^{k_1 c}-e^{-k_1 c}}{2k_1}+\frac{\sinh(k_2 c)}{k_2}\right)$$
$$=\frac{4\pi\sigma_1 v B_{r0}^2}{\tau^2}\left(\frac{e^{k_1 c}-e^{-k_1 c}}{2k_1}+\frac{\sinh(k_2 c)}{k_2}\right)\times \tag{40}$$
$$\left|\frac{\sin\frac{\pi w_m}{2\tau}\sinh\frac{\pi h_m}{\tau}}{\lambda\sinh\frac{\lambda c}{2}\cosh\frac{\pi(2g+c)}{2\tau}+\frac{\pi}{\tau}\cosh\frac{\lambda c}{2}\sinh\frac{\pi(2g+c)}{2\tau}}\right|^2$$

From the above formula, it can be seen that the braking force

density is related to the pole distance, air gap length, permanent magnet thickness, conductor plate thickness and permanent magnet length of the brake. It is noteworthy that the air gap length, the thickness of permanent magnet and the length of permanent magnet all affect the brake force density by the ratio of the air gap to the pole distance. Therefore, the influence of these main structural parameters on brake performance can be studied by combining analytical method and finite element simulation. The same conclusion applies to the braking force generated by the unit permanent magnet

B. The Influence of Pole Numbers on Braking Force

From (37), the pole logarithm has no effect on the brake force density, but the selection of pole logarithm has a direct impact on the brake force fluctuation. Because the secondary conductor plate is finite in length, that is, it starts at both ends along the direction of motion, the eddy current distribution at both ends will be distorted, which will cause fluctuations in brake operation. When the number of brake poles increases, the length of secondary and conductor plate increases correspondingly, and the proportion of eddy current at the two ends of the conductor plate to the total eddy current decreases, which reduces the fluctuation of braking force. Figure 6 below shows the influence curve of the pole number of the brake on the brake force fluctuation rate when the brake is running at 5m/s and the pole distance is constant.

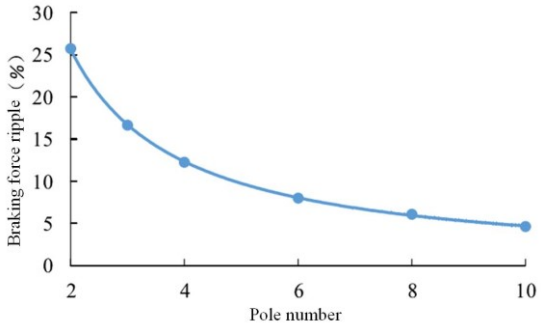

Fig. 6. Influence of pole number on braking force ripple.

As can be seen from the figure above, the influence of pole number on brake force fluctuation rate is more obvious. When pole number is small, the brake force fluctuation rate increases obviously. Therefore, in order to reduce the fluctuation of brake force, the pole number of brake should be increased as much as possible. However, the increase of the pole number of the brake will increase the length of the brake along the direction of motion. In some cases with limited length, it is necessary to consider the trade-off comprehensively. Considering the limitation of brake length, 8 pairs of poles are selected.

C. The Influence of Primary Structural Parameters on Braking Force

Pole distance is an important parameter affecting the performance of permanent magnet linear eddy current brake. It can be seen that other structural parameters mostly affect the braking force density of the brake by the ratio of the pole distance. Therefore, the influence of pole distance on the braking performance of the permanent magnet linear eddy current brake is studied firstly. In order to study the influence of different pole spacing on braking force density, the length of air gap, thickness of permanent magnet, pole arc coefficient and width of conductor plate are kept unchanged. Fig. 7 shows the curve of braking force density varying with pole distance at a series of running speeds.

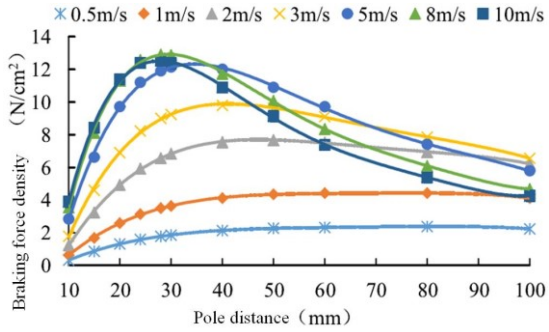

Fig. 7. Influence of pole distance on braking force density.

From the above curves, it can be seen that the pole distance has a great influence on the braking force density. If the pole distance is too small or too large, the braking force density will be reduced. The larger the brake speed is, the smaller the pole distance corresponding to the maximum braking force density is. It can be seen from this that the brake with larger pole distance is suitable for low-speed motion occasions, and the brake with smaller pole distance is suitable for high-speed motion occasions.

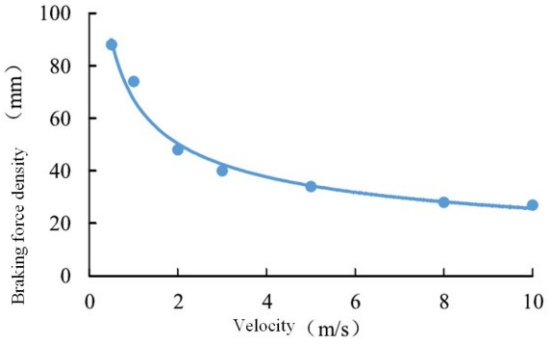

Fig. 8. Optimal pole distance curve.

The optimal pole distance curve of the brake shown in Figure 8 below when the air gap length is 3 mm is obtained by connecting the optimal pole distance at different speeds in Figure 7. In the follow-up study of this section, the parameters of brake speed 5 m/s are studied, and other operating speed states can be given similarly. From Figure8, it can be seen that when the brake speed is 5 m/s, the braking force density is the largest when the pole distance is 34 mm, so the pole distance of the brake is 24 mm.

As an important primary parameter, the length of permanent magnet directly affects the air gap magnetic density and the brake force. It can be seen that the selection of the length of permanent magnet can be carried out by studying the arc coefficient. Fig. 9 below shows the influence of pole arc coefficient on braking force density and unit permanent magnet power; Fig. 10 shows the influence of pole arc coefficient on braking force fluctuation.

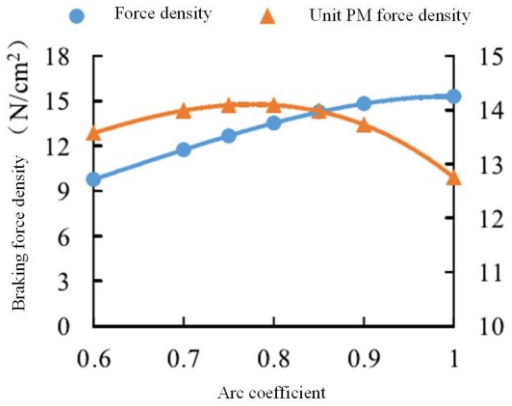

Fig. 9. Influence of arc coefficient on braking force density.

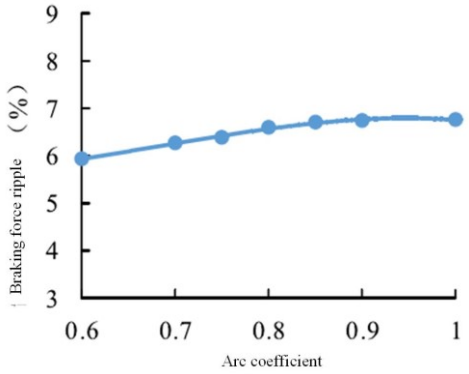

Fig. 10. Influence of arc coefficient on braking force ripple.

From Fig. 9 it can be seen that the greater the arc coefficient, the greater the braking force density of the brake, and the power of the unit permanent magnet system increases first and then decreases. This is due to the increase of pole arc coefficient, that is to say, the length of permanent magnet increases when the pole distance is unchanged, so that the magnetic flux of air gap surface corresponding to a pole distance increases, even if the air gap magnetic density increases, thus increasing the brake force. When the pole arc coefficient is small, the magnetic density of the permanent magnet is small, which leads to the smaller power per unit permanent magnet system. But when the pole arc coefficient is too large, the gap between the adjacent permanent magnets decreases, which leads to the increase of magnetic leakage between the adjacent permanent magnets, and consequently the utilization efficiency of the permanent magnets decreases, and the power per unit permanent magnet system decreases greatly. It can be seen from Figure 10 that the braking force fluctuation increases with the increase of pole arc coefficient, but when the pole arc coefficient is large, the braking force fluctuation increases slowly and the overall change is not obvious. In order to increase the brake force density and ensure the utilization of permanent magnets, the pole arc coefficient of the brake is 0.85, that is, the length of the permanent magnet is 28.9 mm.

Permanent magnet thickness is the length of the permanent magnet along the magnetization direction. Increasing the thickness of permanent magnet will increase the overall thickness of the brake, but also increase the cost of the brake to a certain extent. Therefore, in order to ensure the optimal braking force density, the thickness of permanent magnet should be reduced as much as possible, that is, to improve the utilization efficiency of permanent magnet. It can be generalized to different pole distance selection situations at different speeds according to the ratio of the thickness of permanent magnet to the pole distance after optimizing the thickness of permanent magnet. Fig. 11 below shows the effect of permanent magnet thickness on braking force density and unit permanent magnet power; Fig. 12 shows the effect of permanent magnet thickness on braking force fluctuation.

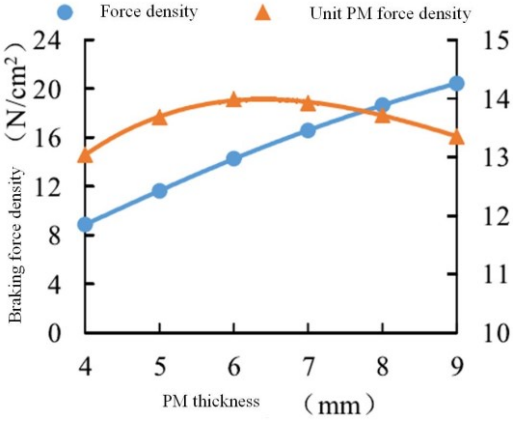

Fig. 11. Influence of PM thickness on braking force density.

From Fig. 11 it can be seen that the greater the thickness of permanent magnet, the greater the brake force density. This is because the increase of the thickness of permanent magnet increases the magnetic momentum in the corresponding magnetic circuit, increases the air gap magnetic density, and then increases the brake force. But with the increase of the thickness of permanent magnet, the power of unit permanent magnet system increases first and then decreases. This is because when the permanent magnet is too thin, the air gap magnetic density is too small and the power of unit permanent magnet system is too small. When the permanent magnet is too thick, the leakage magnetic flux between adjacent permanent magnets increases, which makes the air gap magnetic density not increase proportionally, and consequently leads to the decrease of the utilization ratio of permanent magnet and the power of unit permanent magnet system. Drop. From Fig. 12, it can be seen that the braking force fluctuation decreases with the increase of the thickness of permanent magnet, and the change is more significant. In order to obtain a larger braking force density and ensure a higher utilization efficiency of permanent magnets, the braking force fluctuation is relatively small. The thickness of permanent magnets along the magnetization direction is 7 mm.

Fig. 13 and Fig. 14 shows the effect of primary core thickness on brake force density and brake force fluctuation, respectively. From the figure below, it can be seen that the increase of the thickness of primary core will increase the fluctuation of braking force density and braking force, but when it increases to a certain value, it will not change. From the figure, it can be seen that when the thickness of primary core is greater than 6 mm, the braking force density basically does not change. The primary core provides access for the main magnetic circuit. The thin core thickness will lead to the saturation of the core and the sharp increase of the magneto resistance, which will greatly reduce the air gap magnetic density and the braking force.

When the primary core reaches a certain thickness, the magnetic line will only pass along the core near the permanent magnet, so the increase of the core thickness will not affect the braking force. However, the excessive thickness of the core will lead to the increase of the overall volume and cost of the brake. In the case of unsaturated core, the selection of primary core thickness often depends on the requirements of mechanical conditions.

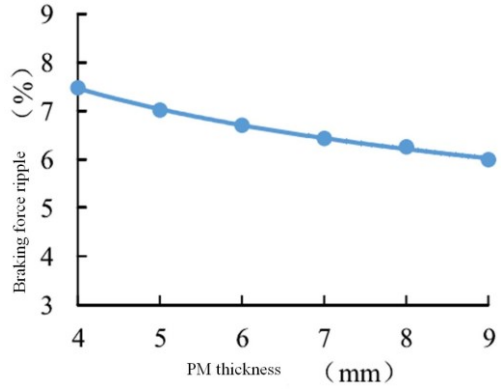

Fig. 12. Influence of PM thickness on braking force ripple.

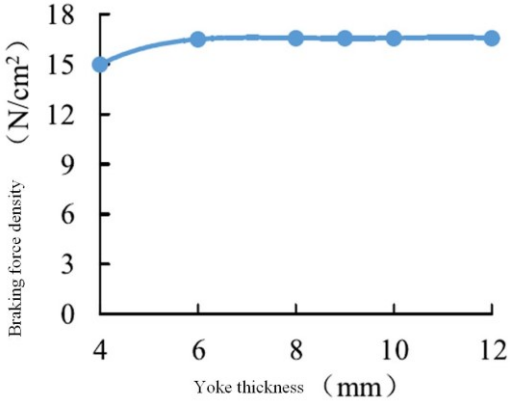

Fig. 13. Influence of yoke thickness on braking force ripple.

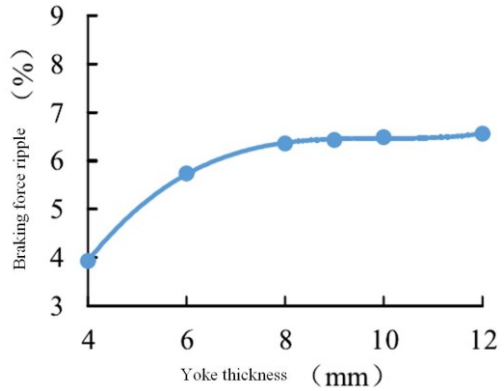

Fig. 14. Influence of yoke thickness on braking force ripple.

D. The Influence of Secondary Structural Parameters on Braking Force

Because the secondary conductor plate is made of non-magnetic material, its permeability is approximately equal to the vacuum permeability, so its thickness determines the size of the electromagnetic air gap of the brake, which has a greater impact on the brake force. Fig. 15 shows the effect of conductor plate thickness on brake force density and brake force fluctuation.

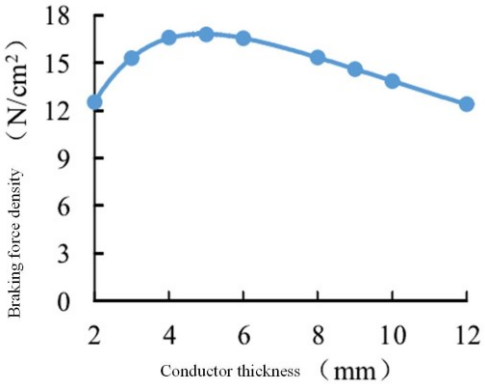

Fig. 15. Influence of conductor thickness on braking force density.

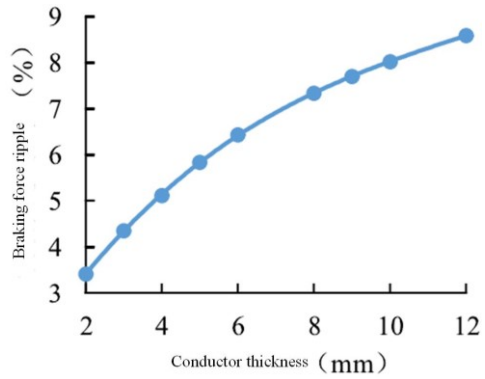

Fig. 16. Influence of conductor thickness on braking force density.

As can be seen from the figure above, the thickness of the conductor plate has a great influence on the braking performance of the brake. With the increase of the thickness of the conductor plate, the brake force density increases first and then decreases; the brake force fluctuation increases gradually, and the increasing trend slows down gradually. When the thickness of the conductor plate is too small, the actual air gap of the brake decreases and the air gap magnetic field increases, but the braking force is smaller due to the thin eddy current layer; when the thickness of the conductor plate increases, the braking force increases accordingly; but when the conductor plate is too thick, the actual air gap magnetic field decreases greatly, and because of the skin-collecting effect, the eddy current divides along the surface layer of the conductor plate. The cloth reduces the braking force. From the graph, it can be seen that the optimal size of the secondary conductor plate of the brake is 4 mm. However, considering the mechanical strength requirements of the secondary plate, 8 mm is chosen here.

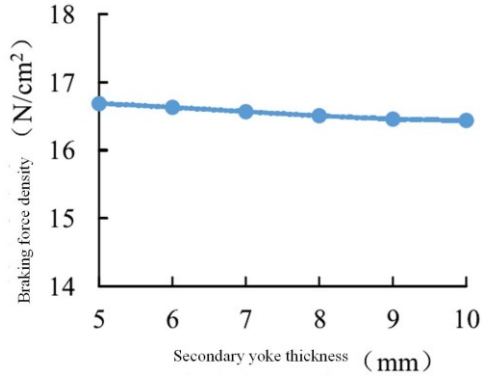

Fig. 17. Influence of secondary yoke thickness on braking force density.

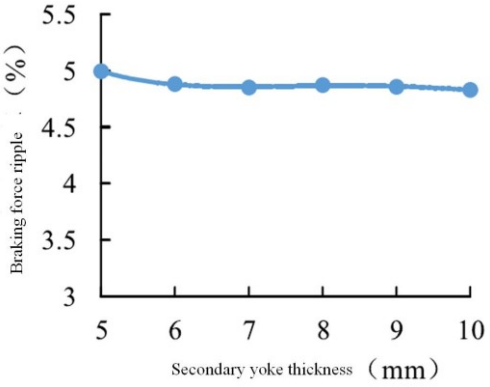

Fig. 18. Influence of secondary yoke thickness on braking force density.

From the previous section, we can know that the optimal thickness of the brake conductor plate is 4 mm. If the secondary of pure aluminum plate takes into account the requirements of mechanical strength, it is necessary to select a thicker secondary plate. But if it is the secondary brake of composite plate, the guide plate with the optimum thickness can be selected. From the analysis above and the comparison with the secondary structure of aluminium plate, it can be seen that the composite secondary structure and the secondary structure of aluminium plate are almost the same in performance, so the thickness of secondary core can be further optimized on the basis of optimizing the secondary structure parameters of aluminium plate. Fig. 17 and Fig. 18 shows the effect of secondary core thickness on brake force density and brake force fluctuation.

As can be seen from the figure, the increase of the thickness of secondary core will make the braking force density decrease slightly, but it has little effect on the fluctuation of the braking force. Considering the braking force density and fluctuation rate, the thickness of secondary core is 6 mm.

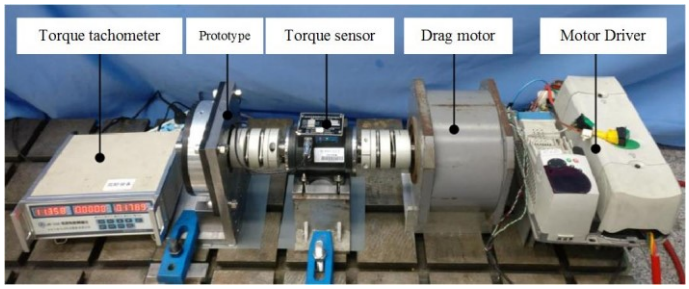

Fig. 19. Test setup.

V. Experimental Study

As the experimental conditions are difficult to achieve, and the rotating structure is considered to replace the linear structure for experimental verification. The experimental prototype is mainly composed of rotating shaft, rotor disc, permanent magnet, front and rear cover, sleeve, rotor key, casing and bearing. The prototype rotor disc, front stator and prototype are shown in Fig. 4-7. One side of the rotor disk is positioned by the shoulder and the other side is positioned by the sleeve to ensure the size of the air gap and prevent the axial movement of the rotor disk when eccentricity occurs. In order to increase the contact area between the rotor key and the rotating shaft and then enhance the connection strength between the rotor key and the rotating shaft, a convex platform is designed to increase the thickness of the bottom rotor disk. The design specifications of the prototype are: pole pitch 34mm, pole pairs 5, air gap length 3mm, magnets inner diameter 78mm, magnets outer diameter 138mm, magnets thickness 7mm, conductor plate outer diameter 150mm, conductor plate thickness 8mm, yoke thickness 15mm, pole arc coefficient 0.85.

In order to verify the braking performance of the permanent magnet eddy current brake and the accuracy of the theoretical method, an experimental platform is built for the prototype to test, as shown in Fig. 19.

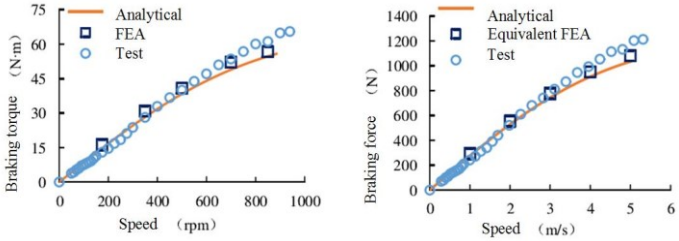

a) Braking torque characteristic b) Equivalent braking force

Fig. 20. Test result.

The experimental platform is mainly composed of a driving motor, a motor driver, a torque sensor, a torque and speed measuring instrument and an experimental prototype. The driving motor, the torque sensor and the prototype are connected by a double diaphragm elastic coupling. The drive motor is a 10-pole permanent magnet synchronous motor, and the position feedback signal is output by a sine-cosine resolver. The driver uses Emerson SP3403 driver to drive the motor at a certain speed. The experimental prototype acts as a brake to provide a constant load for the motor. The speed and torque signals of the experimental system are measured by the torque sensor between the two. Then the braking torque-speed characteristic curve of the experimental prototype can be obtained. The comparison curves of the measured values, the analytical values and the finite element simulation are shown in Fig. 20.

From the figure, it can be seen that the analytical method, finite element method and experimental torque (force) characteristic curve are basically consistent, which verifies the correctness of the analytical model and finite element model. Fig. 20a) shows the comparative curve of the torque characteristics of the prototype. The analytical method is based on the linear brake model, which is affected by the circumferential curvature to a certain extent. Therefore, the analytical value will be slightly different from the experimental value of the prototype. Fig. 20b) shows the comparison of the force characteristic curves of linear brakes. It can be seen that the approximate equivalent method of rotating instead of linear brakes is feasible in a certain range.

VI. Conclusion

As a new type of brake device, permanent magnet eddy current brake overcomes the problems of traditional adhesive

brake device such as contact condition, friction, noise and easy damage. It has the advantages of non-contact, high reliability, high power density and simple structure. It has broad application prospects in the field of braking and vibration suppression. In this paper, the long stroke moving secondary permanent magnet linear eddy current brake is studied. The electromagnetic characteristics of the brake are analyzed and compared by analytical method and finite element method, and the performance of the prototype is tested.

REFERENCES

[1] A. Canova, B. Vusini. "Analytical modeling of rotating eddy-current couplers". *IEEE Transactions on Magnetics*, vol. 41, no. 1, pp. 24-35, 2005.

[2] S. Mohammadi, M. Mirsalim. "Double-sided permanent-magnet radial-flux eddy-current couplers: three-dimensional analytical modelling, static and transient study, and sensitivity analysis". *IET Electric Power Applications*, vol. 7, no. 9, pp. 665-679, 2013.

[3] S. Mohammadi, M. Mirsalim, S. "Vaez-Zadeh. Nonlinear Modeling of Eddy-Current Couplers". *IEEE Transactions on Energy Conversion*, vol. 29, no. 1, pp. 224-231, 2014.

[4] N. Takahashi, M. Natsumeda, K. Muramatsu, et al. "Optimization of permanent magnet type of retarder using 3-D finite element method and direct search method". *IEEE Transactions on Magnetics*,vol. 34, no. 5, pp. 2996-2999, 1998.

[5] L. Ye, D. Li, Y. Ma, et al. "Design and Performance of a Water-cooled Permanent Magnet Retarder for Heavy Vehicles". *IEEE Transactions on Energy Conversion*, vol. 26, no. 3, pp. 953-958, 2011.

[6] A. Canova, B. Vusini. "Design of axial eddy-current couplers". *IEEE Transactions on Industry Applications*, vol. 39, no. 3, pp. 725-733, 2003.

[7] N. Amati, A. Tonoli, A. Canova, et al. "Dynamic Behavior of Torsional Eddy-Current Dampers: Sensitivity of the Design Parameters". *IEEE Transactions on Magnetics*, vol. 43, no. 7, pp. 3266-3277, 2007.

[8] H. Shin, J. Choi, H. Cho, et al. "Analytical Torque Calculations and Experimental Testing of Permanent Magnet Axial Eddy Current Brake". *IEEE Transactions on Magnetics*, vol. 49, no. 7, pp. 4152-4155, 2013.

[9] J. Wang, H. Lin, S. Fang, et al. "A General Analytical Model of Permanent Magnet Eddy Current Couplings". *IEEE Transactions on Magnetic*s, vol. 50, no. 1, pp. 1-9,2014.

[10] T. Lubin, A. Rezzoug. "Steady-State and Transient Performance of Axial-Field Eddy-Current Coupling". *IEEE Transactions on Industrial Electronics*, vol. 62, no. 4, pp. 2287-2296, 2015.

[11] T. Lubin, A. Rezzoug. 3-D "Analytical Model for Axial-Flux Eddy-Current Couplings and Brakes Under Steady-State Conditions". *IEEE Transactions on Magnetics*, vol. 51, no. 10, pp. 1-12, 2015.

[12] M. P. Perry. "Eddy current damping due to a linear periodic array of magnetic poles". *IEEE Transactions on Magnetics*, vol. 20, no. 1, pp. 149-155, 1984.

[13] J. Seok-Myeong, L. Sung-Ho. "Comparison of three types of permanent magnet linear eddy-current brakes according to magnetization pattern". *IEEE Transactions on Magnetics*, vol. 39, no. 5, pp. 3004-3006,2003.

[14] J. S. Choi, J. Yoo. "Optimal design method for magnetization directions of a permanent magnet array". *Journal of Magnetism and Magnetic Materials*, vol. 322, no. 15, pp. 2145-2151, 2010.

[15] H. Bensaidane, T. Lubin, S. Mezani, et al. "A New Topology for Induction Heating System With PM Excitation: Electromagnetic Model and Experimental Validations". *IEEE Transactions on Magnetics*, vol. 51, no. 10, pp. 1-11, 2015.

[16] M. Messadi, L. Hadjout, Y. Ouazir, et al. "Eddy Current Computation in Translational Motion Conductive Plate of an Induction Heater With Consideration of Finite Length Extremity Effects". *IEEE Transactions on Magnetics*, vol. 52, no. 3, pp. 1-4, 2016.

[17] J. Y. Choi and S. M. Jang, "Analytical magnetic torque calculations and experimental testing of radial flux permanent magnet-type eddy currentbrakes," *J. Appl. Phys*., vol. 111, no. 7, pp. 07E712-1–07E712-3, Feb.2012.

[18] N. Amati, A. Tonoli, A. Canova, F. Cavalli, and M. Padovani, "Dynamic behavior of torsional eddy-current dampers: Sensitivity of the design parameters," *IEEE Trans. Magn.*, vol. 43, no. 7, pp. 3266–3277, Jul. 2007.

[19] Z. J. Liu, A. Vourdas, and K. J. Binns, "Magnetic field and eddy current losses in linear and rotating permanent magnet machines with a large number of poles," *IEE Proc.-A,* vol. 138, no. 6, pp. 289–294, Nov. 1991.

[20] R. L. Russell, K. H. Norsworthy. "Eddy currents and wall losses in screened-rotor induction motors". *Proceedings of the IEE Part A: Power Engineering*, vol. 105, no. 20, pp. 163-175, 1958.

Baoquan Kou (M'09) received the B.E. and D.E. degrees from Harbin Institute of Technology (HIT), China, in 1992 and 2004, respectively, and the M.E. degree from Chiba Institute of Technology, Japan, in 1995.

He worked in the mobile station for the post doctors of HIT from 2005 to 2007. Since 2007, he has been a Professor in the School of Electrical Engineering and Automation, HIT. His research interests include electric drive of electric vehicles, linear motors and linear electromagnetic drives, control of the power quality, and superconducting motors.

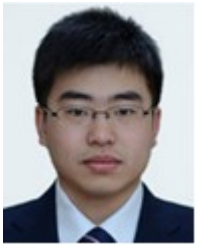

He Zhang received the B.E., M.E. and D.E. degrees from Harbin Institute of Technology, China, in 2008, 2010 and 2015 respectively.

Since 2015, he worked in the Institute of Electromagnetic and Electronic Technology. His research interests include planar motors of high positioning accuracy and high response.

Xiangrui Yin received the B.E. and M.E. degrees from Harbin Institute of Technology, China, in 2015 and 2017 respectively.

His research interests include permanent magnet brakes.

Yiheng Zhou received the B.E. and M.E. degrees in Electrical Engineering from Harbin Institute of Technology, Harbin, China, in 2011 and 2013, respectively, where he is currently working towards the Ph.D. degree in the Institute of Electromagnetic and Electronic Technology.

His research interests include the design and analysis of linear actuators, planar actuators, vibration isolation systems, and electromagnetic brakes.

Chunyan Li received the M.E. and Ph.D. degrees from Harbin Institute of Technology (HIT), China, in 2005 and 2009 respectively.

She is currently with Heilongjiang University. Her research interests include the design of motors and brakes.